Molecular Orbital and Spectroscopic Studies of Triple Bonds between Transition-Metal Atoms. 2. The d^5-d^5 $Re_2Cl_4(PR_3)_4$ Compounds[1]

Bruce E. Bursten,[2a] F. Albert Cotton,*[2a] Phillip E. Fanwick,[2a] George G. Stanley,[2a] and Richard A. Walton[2b]

Contribution from the Departments of Chemistry, Texas A&M University, College Station, Texas 77843, and Purdue University, West Lafayette, Indiana 47907.
Received September 7, 1982

Abstract: The valence electronic structure of compounds containing Re–Re bonds of order 3 and 3.5 has been investigated by using molecular orbital theory and low-temperature electronic absorption spectroscopy. Relativistic Xα-SW calculations have been performed on $Re_2Cl_4(PH_3)_4$ and its cation as models of the well-characterized $Re_2Cl_4(PR_3)_4$ and $[Re_2Cl_4(PR_3)_4]^+$ (R = alkyl) systems. The calculations indicate that the two and one electron(s), respectively, in excess of a quadruple bond reside in the Re–Re δ^* orbital, in agreement with the currently accepted view of bonding in d^5–d^5 dimers and their cations. The Re–P bonding electrons are higher in energy than those in the Re–Cl bonds, but the Re–P bonds are stronger. The substitution lability of the phosphine ligands in the oxidized species is explained on the basis of electrostatic repulsion between the positively charged Re and P centers. The low-temperature spectrum of $Re_2Cl_4(P\text{-}n\text{-}Pr_3)_4$ is reported and a tentative assignment, based on the calculations, is advanced. The spectrum of the oxidized species $[Re_2Cl_4(P\text{-}n\text{-}Pr_3)_4]PF_6$ is also reported. The $\sigma^2\pi^4\delta^2\delta^{*1}$ electron configuration, as expected, gives rise to a $\delta \rightarrow \delta^*$ transition, which is observed in the near-infrared portion of the spectrum. This band exhibits a vibrational progression of frequency 275 ± 5 cm^{-1}, suggesting that the Re–Re bonds in these systems are stronger than that in $[Re_2Cl_8]^{2-}$, despite the greater bond order (4) of the latter.

Following the recognition that the $[Re_2Cl_8]^{2-}$ ion contains a quadruple Re–Re bond,[3] there has been steady growth in the synthesis, structural characterization, and physical description of species containing multiple bonds between metal atoms.[4] While the major theoretical effort has been directed at quantitatively describing the quadruple bonds, because of their intrinsic beauty and seminal role in this field, recent attention has turned to systems containing both lower and higher bond orders.

Of particular interest here are systems containing metal–metal triple bonds, which can be formally derived from the d^4–d^4 quadruple bond by either deleting or adding two electrons (Figure 1). Deletion leads to d^3–d^3 compounds, most prevalent for Mo and W, which formally contain one σ and two π M–M bonds. The description of the electronic structure of d^3–d^3 dimers was the focus of the first paper in this series,[1] as well as of studies by others.[5] In this report we turn to the other class of metal–metal triply bonded systems, namely, the d^5–d^5 dimers in which two electrons have been added to the d^4–d^4 quadruple bond. These electrons populate the δ^* orbital, effectively cancelling the δ bond, leaving a net triple bond, which consists, again, of one σ and two π components. Dinuclear rhenium(II) compounds of general formulation $M_2X_nL_{8-n}$ are by far the most prevalent d^5–d^5 triply bonded dimers generated thus far, with the chemistry of such system having been extensively developed by Walton and coworkers.[6]

The first d^5–d^5 compound to have its structure determined crystallographically was $Re_2Cl_4(PEt_3)_4$,[7] and at the time this was done (1976) the results led to some confusion. The Re–Re distance, 2.232 (6) Å, was not significantly different from that in $Re_2Cl_6(PEt_3)_2$,[8] where there is a quadruple bond and the rotational conformation remained eclipsed. While the eclipsed conformation was recognized to be demanded by nonbonded repulsions and hence not necessarily indicative of any angular bias inherent in the Re–Re bond itself, the Re–Re distance led to an incorrect conclusion. On the basis of what was then known about the bonding in $[Mo_2Cl_8]^{4-}$ and $[Re_2Cl_8]^{2-}$ from SCF Xα-SW calculations,[9] it appeared that if the two additional electrons added to the $\sigma^2\pi^4\delta^2$ set were to enter the δ^* orbital, they would have to cause an increase in the Re–Re distance. Since no increase was found, it was proposed that they entered some other molecular orbital, such as an Re–P antibonding orbital or σ nonbonding orbital composed of 6s and $6p_z$ orbitals of the metal atoms, thus leaving the $\sigma^2\pi^4\delta^2$ quadruple bond intact.

We now know that M–M bond lengths in systems of this type are not simply determined by the δ-bond order because changes in the metal atom charges can alter the strengths of the σ and π components.[10] In the situation we are dealing with here, the addition of two electrons to the δ^* orbital would, by itself, have the effect of weakening and therefore lengthening the bond. However, the decrease in the formal oxidation number of the metal atoms from +3 to +2 will cause an increase in the strengths of the σ and π bonds, thus tending to shorten the distance. In the case of the $Re_2Cl_4(PR_3)_4$ molecules, these two effects almost exactly offset each other and the Re–Re distance is scarcely changed.

In this paper we report relativistic SCF Xα-SW calculations on $Re_2Cl_4(PH_3)_4$ and its cation, which give a detailed picture of their electronic structures and provide support for the descriptions of the bond orders in these as 3 and 3.5, respectively. The modeling of trialkylphosphines by PH_3 would not be expected to cause any serious problem in the interpretation. Additionally, we report and, with the aid of the calculations, assign the low-temperature electronic spectra of $Re_2Cl_4(P\text{-}n\text{-}Pr_3)_4$ and $[Re_2Cl_4(P\text{-}n\text{-}Pr_3)_4]PF_6$. The latter species exhibits vibrational structure in its first band, the frequency of which implies that the Re–Re bond in the excited,

(1) Part 1: Bursten, B. E.; Cotton, F. A.; Green, J. C.; Seddon, E. A.; Stanley, G. G. *J. Am. Chem. Sec.* **1980**, *102*, 4579.
(2) (a) Texas A&M University. (b) Purdue University.
(3) Cotton, F. A. *Inorg. Chem.* **1965**, *4*, 334.
(4) (a) Cotton, F. A.; Walton, R. A. "Multiple Bonds Between Metal Atoms"; Wiley: New York, 1982. (b) Cotton, F. A.; Chisholm, M. H. *Chem. Eng. News* **1982**, *60* (26), 40.
(5) (a) Albright, T. A.; Hoffmann, R. *J. Am. Chem. Soc.* **1978**, *100*, 7736. (b) Hall, M. B. *Ibid.* **1980**, *102*, 2104.
(6) (a) Ebner, J. R.; Walton, R. A. *Inorg. Chem.* **1975**, *14*, 1987. (b) Glicksman, H. D.; Walton, R. A. *Inorg. Chim. Acta* **1976**, *19*, 91. (c) Ebner, J. R.; Tyler, D. R.; Walton, R. A. *Inorg. Chem.* **1976**, *15*, 833. (d) Hertzer, C. A.; Walton, R. A. *Inorg. Chim. Acta* **1977**, *22*, L10. (e) Glicksman, H. D.; Walton, R. A. *Inorg. Chem.* **1978**, *17*, 200. (f) Brant, P.; Walton, R. A. *Ibid.* **1978**, *17*, 2674. (g) Glicksman, H. D.; Walton, R. A. *Ibid.* **1978**, *17*, 3197. (h) Brant, P.; Salmon, D. J.; Walton, R. A. *J. Am. Chem. Soc.* **1978**, *100*, 4424.
(7) Cotton, F. A.; Frenz, B. A.; Ebner, J. R.; Walton, R. A. *Inorg. Chem.* **1976**, *15*, 1630.
(8) Cotton, F. A.; Foxman, B. M. *Inorg. Chem.* **1968**, *7*, 2135.
(9) (a) Norman, J. G., Jr.; Kolari, H. J. *J. Am. Chem. Soc.* **1975**, *97*, 33. (b) Mortola, A. P.; Moskowitz, J. W.; Rosch, N.; Cowman, C. D.; Gray, H. B. *Chem. Phys. Lett.* **1975**, *32*, 283.
(10) Cotton, F. A.; Davison, A.; Day, V. W.; Fredrich, M. F.; Orvig, C.; Swanson, R. *Inorg. Chem.* **1982**, *21*, 1211. See also: Cotton, F. A. *Chem. Soc. Rev.*, in press.

0002-7863/83/1505-2606$01.50/0

Table I. Upper Valence Molecular Orbitals of $Re_2(PH_3)_4Cl_4$ Relativistic Calculation

level[a,b]	energy, eV	% contributions[c] Re	Cl	P	H1	H2	INT	OUT	Re angular contributions[d]			
$9a_1$	−4.133	36	26	1	0	0	29	7	24% s	9% p	67% d	
$8a_1$	−4.569	37	4	25	6	0	26	2	16% s	20% p	63% d	
$8b_2$	−4.743	49	23	8	0	1	17	2	3% p	95% d	2% f	
10e	−5.008	76	7	6	0	1	9	0	96% d	4% f		
$7b_2$	−5.420	54	3	11	4	0	27	1	13% p	85% d	3% f	
$3a_2$	−6.989	80	15	2	0	1	0	1	100% d			
$3b_1$	−7.766	72	21	1	0	1	4	0	100% d			
9e	−9.179	35	25	24	1	3	12	0	20% p	75% d	5% f	
8e	−10.046	26	43	18	1	2	10	0	5% p	89% d	7% f	
$6b_2$	−10.658	5	75	5	1	0	14	0				
$7a_1$	−10.773	2	78	3	2	1	14	0				
$2a_2$	−11.075	10	72	2	0	2	14	0	98% d	2% f		
7e	−11.147	6	61	12	0	4	17	0				
$2b_1$	−11.156	14	63	5	0	7	12	0	100% d			
6e	−11.270	22	59	6	2	0	10	0	24% p	72% d	4% f	
$6a_1$	−11.579	36	5	40	1	9	9	0	11% s	1% p	87% d	2% f
$5b_2$	−11.770	30	6	40	0	11	13	0	26% s	3% p	70% d	1% f
5e	−12.014	32	57	4	3	2	2	0	9% p	85% d	6% f	
$4b_2$	−12.916	1	1	47	36	14	0	0				
$5a_1$	−12.971	2	5	45	33	15	0	0				
4e	−12.976	3	4	45	32	16	0	0				
$1a_2$	−13.074	1	1	47	0	51	0	0				
3e	−13.075	0	1	47	0	51	0	0				
$1b_1$	−13.234	2	4	44	0	47	2	0				
$3b_2$	−13.304	30	70	0	0	0	0	0	27% s	1% p	71% d	1% f
$4a_1$	−13.498	28	62	4	2	0	3	0	44% s	1% p	54% d	1% f
$3a_1$	−15.838	99	0	0	0	0	0	0	20% s	15% p	56% d	9% f

[a] Levels above −4.0 eV are diffuse orbitals with the majority of their charges located in the inter- and outersphere regions and are not listed here. [b] The HOMO is the $3a_2$ level. [c] INT = intersphere and OUT = outersphere charge contributions. [d] Listed only for levels that have 10% or more rhenium contributions.

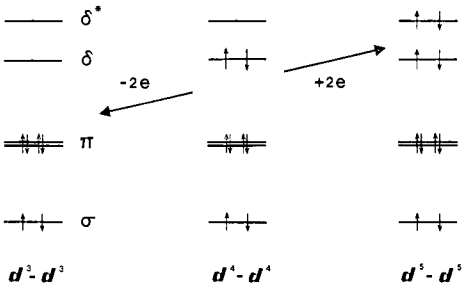

Figure 1. A qualitative MO diagram illustrating the two general types of M–M triple bonds formed by the substraction (d^3–d^3) or addition (d^5–d^5) of two electrons to the d^4–D^4 M–M quadruple bond.

$\sigma^2\pi^4\delta\delta^{*2}$, configuration of this ion is comparable in strength to that in $Re_2Cl_6(PEt_3)_2$.

Computational Section

Bond distances and angles for $Re_2Cl_4(PH_3)_4$ were taken from the crystal structure[7] of $Re_2Cl_4(PEt_3)_4$ and were idealized to D_{2d} symmetry. The bond distances and angles used were the following: Re–Re = 2.232 Å, Re–Cl = 2.360 Å, Re–P = 2.530 Å, P–H = 1.415 Å, Re–Re–Cl = 102.5°, Re–Re–P = 104.1°, and H–P–H = 93.5°. The initial molecular potential was constructed from Re (+2.0), Cl (−0.50), and P (−0.50) Herman–Skillman atomic potentials[11] and H 1s radial functions. The sphere radii used were the following: Re = 2.731 51 au, Cl = 2.5653 au, P = 2.3671 au, H = 1.4226 au, and the outer-sphere = 10.5364 au. The partial wave basis consisted of s-, p-, d-, and f-type spherical harmonics on the Re aotms, s, p, and d on the P and Cl_4 atoms, s only on the H atoms, and up through $l = 8$ on the outer sphere.

The nonrelativistic SCF calculation was started by using a 5% mixing of the new potential into the old to generate the starting potential for the next iteration. The mixing was eventually increased to a maximum of 15%. After 10 interations the relativistic valence and core corrections[12] on the rhenium atomic potential were included and mixed in over 10 more iterations. A total of 60 iterations were required to reach convergence with a typical relativistic iteration requiring ca. 40-s execution time. Because of the expected low energy of the HOMO's, a Watson sphere[13] with a charge of +1.0 and a radius 1 au greater than the outer sphere was used to stabilize the energy levels.

The calculation on the cation $[Re_2Cl_4(PH_3)_4]^+$ was performed by taking the converged potential deck from the $Re_2Cl_4(PH_3)_4$ calculation, removing one electron from the HOMO and reconverging the calculation. The Watson sphere was not necessary for this calculation and was removed. After convergence, the potential and energy levels were made spin-unrestricted and reconverged.

Experimental Section

$Re_2Cl_4(Pn\text{-}Pr_3)_4$ and $[Re_2Cl_4(Pn\text{-}Pr_3)_4]PF_6$ were prepared by previously established methods.[6a,b] KBr pellets of these were prepared under N_2. Low-temperature electronic spectra were measured on a Cary 17D spectrophotometer using a previously described[14] cryogenic and computer system.

Results and Discussion

$Re_2Cl_4(PH_3)_4$. The results of the relativistic SCF Xα-SW calculation on $Re_2Cl_4(PH_3)_4$ are presented in Table I, and are compared to our previous calculation[15] on $[Re_2Cl_8]^{2-}$ in Figure 2. The HOMO of the complex is the $3a_2$ molecular orbital, which has axial δ^* symmetry, and lies ca. 0.8 eV above the $3b_1$ δ molecular orbital. Contour plots of these two orbitals along the dihedral plane of the molecule are presented in Figure 3. It is apparent that these calculations support the formulation of the Re–Re bond in the Re_2^{4+} species as a $\sigma^2\pi^4\delta^2\delta^{*2}$ configuration, resulting in a net triple bond with no δ component. The earlier suggestions that Re–P antibonding or σ-nonbonding orbitals might be occupied rather than the δ^* orbital are invalidated by this calculation.

In $Re_2Cl_4(PH_3)_4$ four e orbitals, namely, the 9e, 8e, 6e, and 5e, all contribute significantly to the Re–Re π bond. This contrasts

(11) Herman, F.; Skillman, S. "Atomic Structure Calculations"; Prentice-Hall: Englewood Cliffs, NJ, 1963.
(12) Wood, J. H.; Boring, M. A. *Phys. Rev. B* **1978**, *18*, 2701.
(13) Watson, R. E. *Phys. Rev.* **1958**, *111*, 1108.
(14) Cotton, F. A.; Fanwick, P. E. *J. Am. Chem. Soc.* **1979**, *101*, 5252.
(15) Bursten, B. E.; Cotton, F. A.; Fanwick, P. E.; Stanley, G. G. *J. Am. Chem. Soc.*, in press.

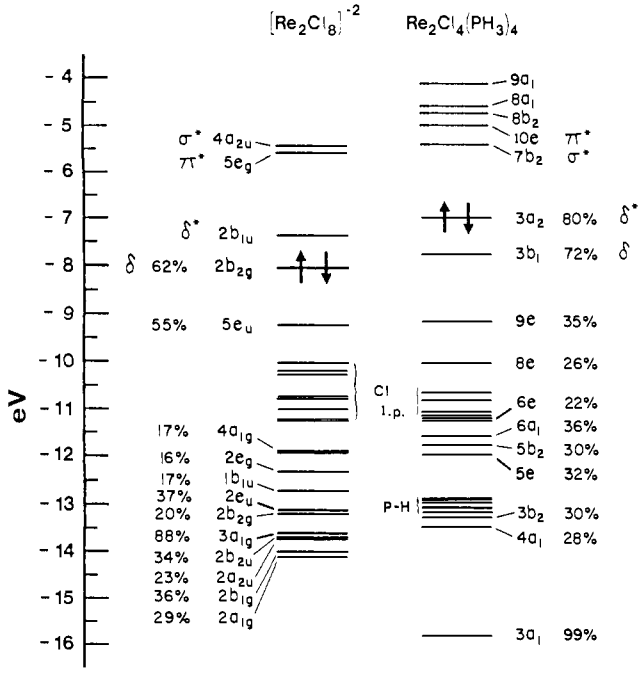

Figure 2. Energy level diagram comparing the relativistic Xα-SW calculations on $[Re_2Cl_8]^{2-}$ [15] and $Re_2Cl_4(PH_3)_4$. The highest occupied molecular orbitals are indicated by arrows. The percent characters are given for occupied levels only and refer to Re atomic sphere charge contributions to each MO which has >10% Re character. The diagram for $[Re_2Cl_8]^{2-}$ has been shifted to match energetically the lowest Cl lone-pair orbital.

with the bonding situation in the relativistic Xα-SW calculation on $[Re_2Cl_8]^{2-}$, where the Re–Re π bonding is concentrated primarily in two e_u orbitals, of which the upper one is Re–Cl antibonding and has 55% Re character, while the lower is Re–Cl bonding with 37% Re character.[15] In $Re_2Cl_4(PH_3)_4$, however, the presence of two sets of rather different ligands causes a further fragmentation of these Re–Re bonding components. The 9e orbital is Re–Re π bonding, Re–Cl π* and Re–P σ* antibonding with equal chlorine and phosphorus (~24% each) contributions. The Re–P σ* (and to a lesser extent, the Re–Cl π*) character is reduced somewhat by the presence of Re 6p character which mixes in with the d_{xz}, d_{yz} AO's reducing the M–L antibonding and improving the Re–Re bonding. There is considerable bonding interaction between the phosphorus atoms and the Re–Re π-bonding orbital lobes which also contributes to the reduction of the Re–P antibonding interaction. The 8e MO is Re–Cl π* antibonding but Re–Re π and Re–P σ bonding. The Re–P σ bonding in the 8e level is similar in magnitude to the Re–P σ* character in the 9e orbital; the two roughly balance each other, resulting in an overall nonbonding Re–P interaction for the 8e and 9e orbitals taken together. The Re–Cl character, however, is π* antibonding, analogous to that seen in the $5e_u$ orbital in $[Re_2Cl_8]^{2-}$. The 6e and 5e orbitals are M–M π and M–L σ bonding with the chlorine atoms the main contributors. Summarizing the bonding in the e levels it is found that they are all Re–Re π bonding and have a total M–L interaction that is only weakly bonding.

The $3a_1$ orbital that provides the Re–Re σ-bonding level is virtually pure rhenium in character (20% 6s, 15% $6p_z$, 56% 5d, and 9% 5f) and occurs about 2.5 eV lower in energy than the $4a_1$ MO. The σ/σ* gap in $Re_2Cl_4(PH_3)_4$ ($3a_1$ to $7b_2$) is, somewhat surprisingly, about 2 eV greater than that in $[Re_2Cl_8]^{2-}$ ($3a_{1g}$ to $4a_{2u}$), implying a stronger Re–Re σ-bonding component in $Re_2Cl_4(PH_3)_4$.[16] As the metal–metal π-bonding interactions between

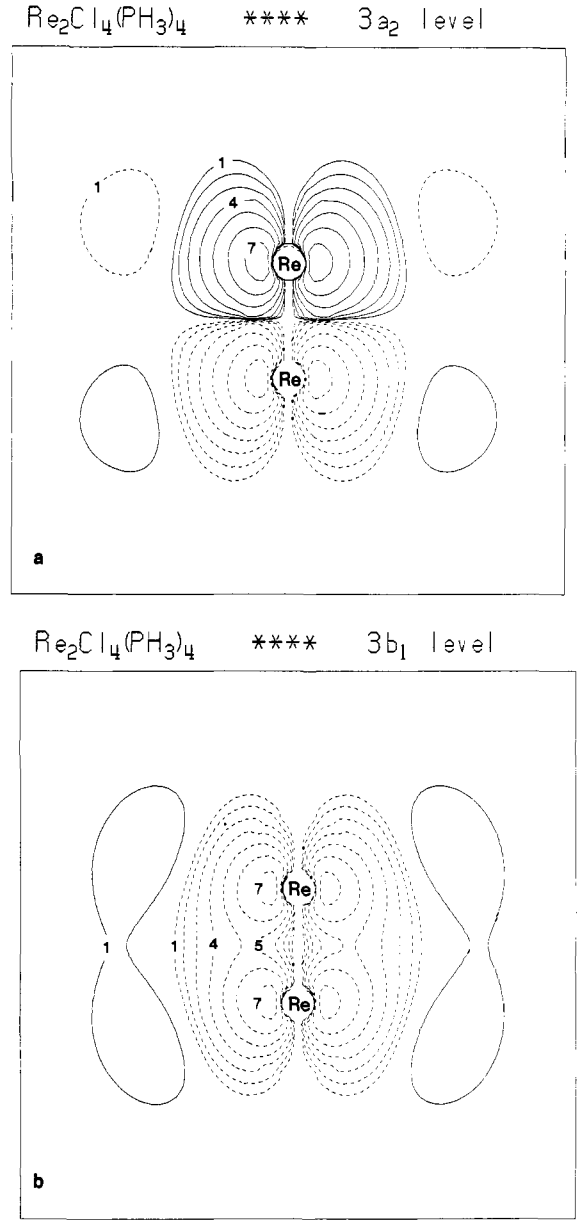

Figure 3. Contour plots of the $3a_2$ (a) and $3b_1$ (b) orbitals of $Re_2Cl_4(PH_3)_4$. Dashed lines indicate negative contour values. Contour values are as follows: ±1 = 0.0025, ±2 = 0.005, ±3 = 0.010; ±4 = 0.020; ±5 = 0.040; ±6 = 0.080; ±7 = 0.160 e/Å^3.

the two are similar, the evaluation of the relative M–M bond strengths depends upon the comparison of the increase in the Re–Re σ bonding vs. the loss of δ bonding in $Re_2Cl_4(PH_3)_4$. Since the δ-bonding interaction is quite weak compared to the σ component,[18] the Re–Re bonding in $Re_2Cl_4(PH_3)_4$ is expected to be at least as strong as, and probably stronger than, that in $[Re_2Cl_8]^{2-}$. Spectroscopic evidence supporting this contention will be presented later in this paper.

The main M–L σ-bonding levels in $Re_2Cl_4(PH_3)_4$ are the $6a_1$, $4a_1$, $5b_2$, and $3b_2$ MO's, which are also split into two distinct classes corresponding to Re–P and Re–Cl σ bonding. The $6a_1$ and $5b_2$ MO's are the Re–P σ-bonding levels with the metal contributions arising primarily from the Re $d_{x^2-y^2}$ AO's with a minor Re d_{z^2}

(16) The size of the Re atomic sphere used in the $Re_2Cl_4(PH_3)_4$ calculation is ca. 0.2 au larger than that used in the $[Re_2Cl_8]^{2-}$ calculation owing to the unusually long Re–P bond. This could cause an overestimation of the σ-orbital stabilization in the former since charge is double counted in the overlap region.[17]

(17) Herman, F.; Williams, A. R.; Johnson, K. H. *J. Chem. Phys.* **1974**, *61*, 3508.

(18) The W–W bond lengths in d^3–d^3 triple-bonded dimers of tungsten are very similar to those in W–W quadruple bonds,[19] suggesting that for third-row metals the δ-bonding component contributes very little to the short M–M bond lengths.

(19) (a) Cotton, F. A. *Acc. Chem. Res.* **1978**, *11*, 225. (b) Collins, D. M.; Cotton, F. A.; Koch, S.; Millar, M.; Murillo, C. *J. Am. Chem. Soc.* **1977**, *99*, 1259.

Table II. Calculated and Experimental Transition Energies (cm^{-1}) for $Re_2Cl_4(PR_3)_4$[a]

orbital transition	type	dipole[b]	OED[c]	exptl[d]
				12 270 (sh)
$3a_2 \rightarrow 7b_2$	$\delta^* \rightarrow \sigma^*$		12 660	13 790
$3a_2 \rightarrow 10e$	$\delta^* \rightarrow \pi^*$	A	15 977	15 460
$3a_2 \rightarrow 8b_2$	$\delta^* \rightarrow$ [Re-L]*		18 114	16 720 (sh)
$3b_1 \rightarrow 7b_2$	$\delta \rightarrow \sigma^*$		18 924	18 830
$3a_2 \rightarrow 8a_1$	$\delta^* \rightarrow$ [Re-P]*		19 520	
$3b_1 \rightarrow 10e$	$\delta \rightarrow \pi^*$	A	22 247	20 620
$3a_2 \rightarrow 9a_1$	$\delta^* \rightarrow$ [Re-Cl]*		23 039	
$3b_1 \rightarrow 8b_2$	$\delta \rightarrow$ [Re-L]*		24 381	24 330
$3b_1 \rightarrow 8a_1$	$\delta \rightarrow$ [Re-P]*		25 787	
$3b_1 \rightarrow 9a_1$	$\delta \rightarrow$ [Re-Cl]*		29 306	28 170 (sh)
$9e \rightarrow 7b_2$	LMCT	A	30 326	strong absorbance
$9e \rightarrow 10E$	LMCT	A	33 641	starting around 30 000

[a] Calculated values are for $Re_2Cl_4(PH_3)_4$. Experimental are for $Re_2Cl_4(P\text{-}n\text{-}Pr_3)_4$ at 5 K in a KBr pellet. [b] A: transition is electric dipole allowed under D_{2d} symmetry. [c] OED: orbital energy difference. [d] sh: shoulder.

contribution to each one. The $3b_2$ and $4a_1$ orbitals are the Re–Cl σ-bonding levels with analogous Re atomic contributions. The difference in bonding and electronegativities between the chlorine and phosphine ligands is enough to cause a separation of these M–L orbitals into two sets, viz., the higher energy Re–P and the lower energy Re–Cl bonding MO's. The higher energy of the phosphine levels results from the lower electronegativity of P and not from any greater strength of the Re–Cl bonding. Indeed, the larger Re contributions in the Re–P bonding orbitals coupled with the greater Re 6p occupations relative to $[Re_2Cl_8]^{2-}$ point to better σ donation from the phosphine ligands to the rhenium atoms, and the Re–P bonding is expected to be somewhat stronger than the Re–Cl bonding.

The prediction of greater phosphine σ donation and hence stronger Re–P bonding is consistent with both the lower electronegativity of the phosphines and the reaction chemistry of dirhenium(II, III) systems. $[Re_2Cl_8]^{2-}$ reacts quantitatively with most phosphines, forming $Re_2Cl_6(PR_3)_2$, $Re_2Cl_5(PR_3)_3$, and $Re_2Cl_4(PR_3)_4$.[6a,20] The steric bulk of the phosphine ligands plays an important role in determining how far the substitution process will go. A large phosphine such as PPh_3 will react with $[Re_2Cl_8]^{2-}$ forming only $Re_2Cl_6(PPh_3)_2$. PPh_2Et will react further forming $Re_2Cl_5(PPh_2Et)_3$, with $PPhEt_2$ going one more step yielding $Re_2Cl_4(PPhEt_2)_4$.[6a] $Re_2Cl_6(PR_3)_2$ compounds can be synthesized under mild conditions with most phosphines. The addition of excess phosphine and/or mild heating affords $Re_2Cl_5(PR_3)_3$ if the PR_3 ligand is large enough to block further reaction, otherwise the process continues and $Re_2Cl_4(PR_3)_4$ compounds are formed.[6a]

The crystal structure of $Re_2Cl_6(PEt_3)_2$ offers further support for stronger phosphine vs. chlorine σ donation and bonding.[9] A 0.05-Å lengthening of the Re–Cl bond distance trans to the phosphine ligands is observed, demonstrative of the trans effect induced by the stronger phosphine coordination and σ donation. As was the case for $Rh_2(O_2CH)_4(PH_3)_2$,[21] there is very little phosphorus 3d mixing in any of the occupied Re–P bonding or antibonding levels, despite the fairly high electron density on the rhenium atoms; thus, the Re–P interaction is a simple σ-donation effect. In light of the experimental and theoretical data, we propose that the fairly long Re–P bond distance in $Re_2Cl_4(PEt_3)_4$ (Re–P = 2.53 (3) Å, which is ~0.08 Å longer than in $Re_2Cl_6(PEt_3)_2$) is caused by steric factors and not by an intrinsic weakness of the Re–P bond. Additional support for this hypothesis is provided by structural studies on the isoelectronic compound $Re_2Cl_4(dppe)_2$, where, because of the lesser steric demands of the dppe ligands, the average Re–P bond distance drops to 2.438 (15) Å.[22]

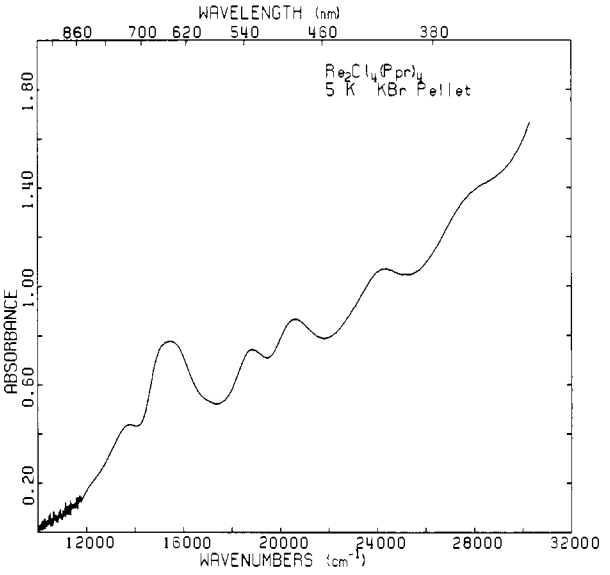

Figure 4. Electronic absorption spectrum of a KBr pellet of $Re_2Cl_4(P\text{-}n\text{-}Pr_3)_4$ at 5 K. No transitions were observed below 11 000 cm^{-1}.

The electronic absorption spectrum of $Re_2Cl_4(P\text{-}n\text{-}Pr_3)_4$ in a KBr pellet at 5 K is shown in Figure 4. The calculated and experimental transition energies are listed in Table II. The lowest calculated transition is $3a_2 \rightarrow 7b_2$ ($\delta^* \rightarrow \sigma^*$) at 12 660 cm^{-1}. The first transition seen in the spectrum of $Re_2Cl_4(PPr_3)_4$ is a weak shoulder at 12 270 cm^{-1} followed by peaks of increasing intensity at 13 790 and 15 460 cm^{-1}. Although the position of the first calculated transition and the low-energy shoulder agree well, we prefer to assign the second absorption at 13 790 cm^{-1} as the dipole forbidden $3a_2 \rightarrow 7b_2$ ($\delta^* \rightarrow \sigma^*$) transition and the relatively strong absorption at 15 460 cm^{-1} as the allowed $3a_2 \rightarrow 10e$ ($\delta^* \rightarrow \pi^*$) excitation. The low-energy shoulder at 12 270 cm^{-1} is tentatively assigned as the triplet component of the $3a_2 \rightarrow 10e$ transition. Relativistic spin-unrestricted transition-state calculations on the $3a_2 \rightarrow 10e$ transition yield a singlet–triplet separation of 3900 cm^{-1}, which agrees well with the position of the low-energy shoulder. The low intensity of this transition ($\epsilon \sim 10$ M^{-1} cm^{-1} based on the $\delta^* \rightarrow \pi^*$ extinction coefficient of 138 M^{-1} cm^{-1} for $Re_2Cl_4(PPr_3)_4$ in benzene),[6a] the greater intensity of the other forbidden singlet transitions in the spectrum, and lack of any other calculated low-energy excitations combine to make this assignment plausible.

The shoulder at 16 720 cm^{-1} is assigned as the forbidden $3a_2 \rightarrow 8b_2$ transition from the Re–Re δ^* orbital to a Re–P σ^*-antibonding level. The calculated energy is too high (18 114 cm^{-1} vs. 16 720 cm^{-1} observed), as is the case in several of the proposed assignments, perhaps due to the smaller donor ability of the model ligand PH_3 relative to P-*n*-Pr_3. The peak at 18 830 cm^{-1} is assigned as the dipole-forbidden $3b_1 \rightarrow 7b_2$ ($\delta \rightarrow \sigma^*$) transition, which, as with the $\delta^* \rightarrow \sigma^*$ transition, possesses enough intensity to be clearly resolved. The absorption at 20 620 cm^{-1} is assigned to the $3b_1 \rightarrow 10e$ ($\delta \rightarrow \pi^*$) transition, which is allowed in D_{2d} symmetry. The broader band at 24 330 cm^{-1} is assigned as any or all of the forbidden $3a_2 \rightarrow 9a_1$, $3b_1 \rightarrow 8b_2$, and $3b_1 \rightarrow 8a_1$ transitions to M–L antibonding orbitals. The shoulder at 28 170 cm^{-1} may be assigned to the $3b_1 \rightarrow 9a_1$ excitation falling on the intense $9e \rightarrow 7b_2$, 10e LMCT transitions, which begin around 30 000 cm^{-1} and continue on into the UV. Therefore, the visible absorption spectrum is composed of a considerable number of transitions from the Re–Re δ^* and δ MO's to the σ^*, π^*, and M–L antibonding virtual levels. These are all fairly weak absorptions which is not surprising since most of the transitions are dipole forbidden. Even the $\delta^* \rightarrow \pi^*$ and $\delta \rightarrow \pi^*$ transitions which are formally allowed in D_{2d} symmetry are expected to be fairly weak because of the low transition moments for excitations between δ- and π-type

(20) (a) Cotton, F. A.; Curtis, N. F.; Robinson, W. R. *Inorg. Chem.* **1965**, *4*, 1696. (b) San Filippo, J., Jr. *Ibid.* **1972**, *11*, 3140.
(21) Bursten, B. E.; Cotton, F. A. *Inorg. Chem.* **1981**, *20*, 3042.
(22) Cotton, F. A.; Stanley, G. G.; Walton, R. A. *Inorg. Chem.* **1978**, *17*, 2099.

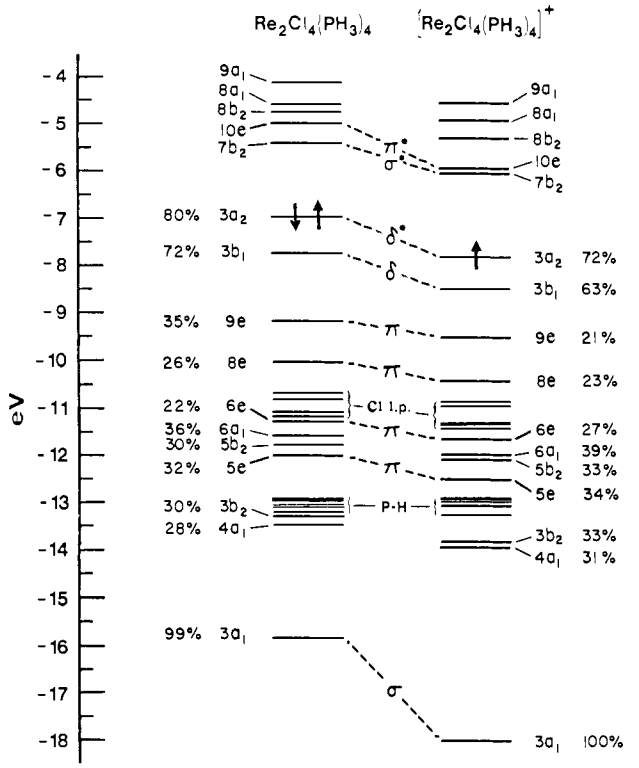

Figure 5. Energy level diagram comparing the relativistic Xα-SW calculations on $Re_2Cl_4(PH_3)_4$ and $[Re_2Cl_4(PH_3)_4]^+$. The notes for Figure 2 apply except that the levels for $[Re_2Cl_4(PH_3)_4]^+$ have been shifted to energetically match the P–H bonding orbitals.

orbitals; these transitions become entirely forbidden under D_{4h} symmetry.

$[Re_2Cl_4(PH_3)_4]^+$. An intense band was observed in the near IR in the solution spectra of $Re_2Cl_4(PR_3)_4$ compounds reported by Walton and co-workers.[6a] The disappearance of this peak in rigorously prepared oxygen-free solutions led Walton to assign it, in analogy with the related $Re_2Cl_5(PR_3)_3$ compounds, to the $\delta \rightarrow \delta^*$ transition in the oxidized species $[Re_2Cl_4(PR_3)_4]^+$. Recently Walton has reported the electrochemistry, synthesis, and isolation of a number of $[Re_2Cl_4(PR_3)_4]^+PF_6^-$ compounds.[6h] In order to investigate the electronic structure of these cationic species, particularly the absorption spectrum, we have carried out spin-restricted and unrestricted relativistic Xα-SW calculations on $[Re_2Cl_4(PH_3)_4]^+$ and have measured the KBr pellet spectrum of $[Re_2Cl_4(P\text{-}n\text{-}Pr_3)_4]^+PF_6^-$ at 5 K. The spin-restricted Xα-SW results are compared to those of $Re_2Cl_4(PH_3)_4$ in Figure 5. Since the various aspects of the M–M and M–L bonding have been discussed in detail in the previous section, we will concentrate here on the differences between the two calculations.

As can be seen in Figure 5, the removal of an electron from the δ^* orbital causes no significant reorganization or change in the bonding character for any of the levels. One rather clear feature is that levels with metal contributions have shifted down in energy more than those that are primarily ligand-based with the relative amount of stabilization roughly proportional to the amount of metal character present in the MO. Correspondingly, the $3a_1$ Re–Re σ-bonding orbital with a 100% Re contribution shows the largest drop, followed by the δ and δ^* orbitals. The Re–L bonding levels show only moderate stabilizations relative to the pure ligand levels. The virtual orbitals show similar trends. Clearly, the removal of an electron from a metal-localized orbital (the δ^*) with the resultant stabilization induced by the greater positive charge also localized on the metal atoms has a greater effect on MO's with substantial metal contributions. The changes in the rhenium contributions in the various M–L bonding MO's are also directly related to the higher effective oxidation state of the Re atoms which lowers the "empty" $d_{x^2-y^2}$ orbitals, allowing an increased M–L interaction as indicated by the greater Re character in the a_1 and b_2 Re–L bonding orbitals. The same

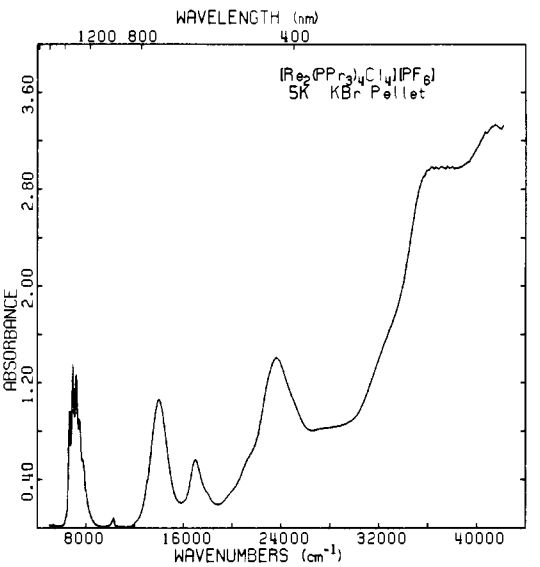

Figure 6. Electronic absorption spectrum of a KBr pellet of $[Re_2Cl_4(P\text{-}n\text{-}Pr_3)_4]PF_6$ at 5 K. The small feature at 10000 cm^{-1} is due to the shift from infrared to visible light sources.

lowering of the occupied d_{xz}, d_{yz} orbitals that are below the ligand levels (particularly those of the phosphine) reduces the Re–L interactions of the 8e and 9e orbitals.

While the greater ligand-to-metal σ donation will favor the M–L bonding somewhat, another factor will work to preferentially destabilize the Re–P bonding. Donation of electron density from the neutral phosphine ligand to the metal results in a positive charge being generated on the phosphine, particularly since no M–P π back-donation to compensate for this charge donation is observed. On removal of an electron from the δ^* orbital the resulting positive charge is localized mainly on the rhenium atoms. The electrostatic repulsions between the positively charged phosphines and rhenium atoms will be increased over that in the neutral complex and will work to weaken the Re–P bonding while making Re–Cl bonding more stable. While our calculations do not show directly what the net effect will be, the electrochemistry of these systems strongly suggests that the electrostatic factor prevails, since the electrochemical oxidation of $Re_2Cl_4(PR_3)_4$ or $Re_2Cl_5(PR_3)_3$ compounds in the presence of chloride ions leads to virtually instantaneous substitution of the necessary phosphines to yield the neutral species $Re_2Cl_6(PR_3)_2$.[6h] The relatively small separation of the δ and δ^* orbitals in the Xα-SW calculations is consistent with the occurrence of facile electrochemical oxidations and reductions that interconvert the $Re_2Cl_6(PR_3)_2^{1-,2-}$, $Re_2Cl_5(PR_3)_3^{1+,1-}$, and $Re_2Cl_4(PR_3)_4^{1+,2+}$ species, all of which possess various δ^* occupations (0–2).[6h] The larger $\delta^* - \sigma^*$ and $\delta - \pi$ separations are also consistent with the lack of any reductions in $Re_2Cl_4(PR_3)_4$ and oxidations in $Re_2Cl_6(PR_3)_2$.

The electronic absorption spectrum of $[Re_2Cl_4(PPr_3)_4]^+$ is presented in Figure 6. The calculated and experimental transition energies are listed in Table III. The calculated values are ordered to coincide with their assigned experimental transitions. The lowest energy absorption occurring at 6653 cm^{-1} is quite intense and is assigned as the fully allowed (in both D_{2d} and D_{4h}) $\delta \rightarrow \delta^*$ excitation. Vibrational fine structure based on the excited-state Re–Re a_1 stretching frequency is clearly seen in the expanded view of the $\delta \rightarrow \delta^*$ band in Figure 7. The average Re–Re stretching frequency from the vibrational progression is 275 ± 5 cm^{-1}. The next absorption at 13072 cm^{-1} is a weak shoulder and is assigned as the forbidden $3a_2 \rightarrow 7b_2$ ($\delta^* \rightarrow \sigma^*$) transition. The strong absorption at 14025 cm^{-1} can confidently be assigned as the allowed $9e \rightarrow 3a_2$ (LMCT) transition which is expected to have a high intensity. The peak at 17036 cm^{-1} is the $3a_2 \rightarrow 10e$ ($\delta^* \rightarrow \pi^*$) allowed excitation which is shifted to higher energies relative to that in the neutral compound. The shoulders at 18018, 19802, and 21510 cm^{-1} are assigned to the $3a_2 \rightarrow 8b_2$ and $3b_1 \rightarrow 7b_2$, 10e orbital transitions. The similarity of the extinction

Table III. Calculated and Experimental Transition Energies (cm^{-1}) for $[Re_2Cl_4(PR_3)_4]^+$

transition	type	dipole[a]	calcd[b] SR	calcd[b] SU	exptl[c]
$3b_1 \rightarrow 3a_2$	$\delta \rightarrow \delta^*$	A	5 540	5 650	6 653
$3a_2 \rightarrow 7b_2$	$\delta^* \rightarrow \sigma^*$		14 450	15 260	13 072 (sh)
$9e \rightarrow 3a_2$	LMCT	A	13 520	14 240	14 025
$3a_2 \rightarrow 10e$	$\delta^* \rightarrow \pi^*$	A	15 270	15 280	17 036
$3a_2 \rightarrow 8b_2$	$\delta^* \rightarrow$ [Re-L]*		20 400	20 070	18 018 (sh)
$3b_1 \rightarrow 7b_2$	$\delta \rightarrow \sigma^*$		19 990	20 330	19 802 (sh)
$3b_1 \rightarrow 10e$	$\delta \rightarrow \pi^*$	A	20 810	20 330	21 510 (sh)
$8e \rightarrow 3a_2$	LMCT	A	20 980	21 580	23 697
$3a_2 \rightarrow 8a_1$	$\delta^* \rightarrow$ [Re-P]*		23 370	23 760	25 000 to 30 000
$6b_2 \rightarrow 3a_2$	LMCT		24 480	25 260	
$7a_1 \rightarrow 3a_2$	LMCT		25 150	25 970	
$3b_1 \rightarrow 8b_2$	$\delta \rightarrow$ [Re-L]*		25 950	25 940	
$3a_2 \rightarrow 9a_1$	$\delta^* \rightarrow$ [Re-Cl]*		26 460	26 880	
$9e \rightarrow 7b_2$	LMCT	A	27 970	28 290	33 330 (sh)
$7e \rightarrow 3a_2$	LMCT	A	28 110	28 910	strong absorption 34 000 and up
$9e \rightarrow 10e$	LMCT	A	28 790	28 290	

[a] A: transition is dipole allowed under D_{2d} symmetry. [b] Calculated transition energies for $[Re_2Cl_4(PH_3)_4]^+$; SR = spin restricted orbital energy difference; SU = spin-unrestricted orbital energy difference. [c] KBr pellet of $[Re_2Cl_4(P\text{-}n\text{-}Pr_3)_4]^+PF_6^-$ at 5 K.

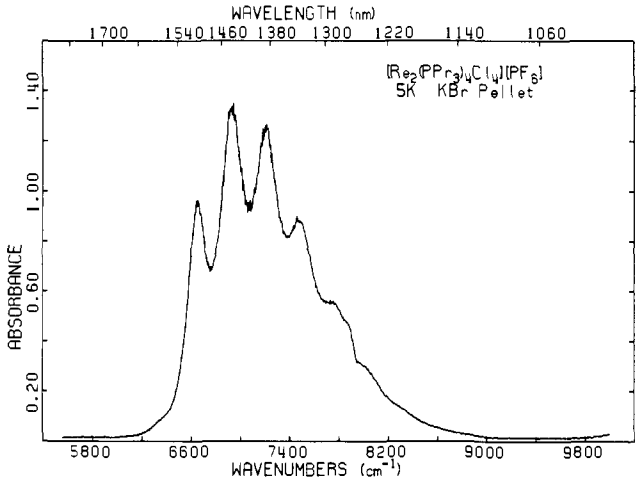

Figure 7. Expanded view of the $\delta \rightarrow \delta^*$ transition in $[Re_2Cl_4(P\text{-}n\text{-}Pr_3)_4]PF_6$.

coefficients of the first two bands is consistent with the forbidden nature of the assigned orbital excitations, while the increased intensity of the 21 510-cm^{-1} shoulder is consistent with the D_{2d} allowed character of the $3b_1 \rightarrow 10e$ transition. The strong absorbance at 23 697 cm^{-1} is caused by the $8e \rightarrow 3a_2$ (LMCT) allowed transition, similar to the $9e \rightarrow 3a_2$ transition at 14 027 cm^{-1}. The shoulder at ~25 000 cm^{-1} and flat portion of the spectrum centered at 28 000 cm^{-1} are assigned to the forbidden $3a_2 \rightarrow 8a_1$ through $3a_2 \rightarrow 9a_1$ transitions listed in Table III, with strong LMCT bands beginning at ~32 000 cm^{-1} and increasing into the UV. Thus, as expected, the main differences between the spectra of $Re_2Cl_4(PR_3)_4$ and $[Re_2Cl_4(PR_3)_4]^+$ arise from the presence of allowed low-energy δ and LMCT transitions into the half-filled δ^* orbital.

As with the $Re_2Cl_4(PH_3)_4$ calculation, the Xα results for $[Re_2Cl_4(PH_3)_4]^+$ have been regarded as a flexible guide in assigning the spectral features. While we feel that the proposed assignments are quite reasonable, we fully recognize the somewhat ad hoc nature of the process as well as the lack of hard experimental evidence for many of the peak assignments, particularly the weak bands. However, without the calculations it is clear that no defensible assignments (aside from the obvious $\delta \rightarrow \delta^*$) could have been made.

All of the calculated energies given in Tables II and III are simple orbital energy differences (OED's) and are not from transition-state calculations. Two spin-unrestricted transition-state calculations were performed on the $3a_2 \rightarrow 10e$ and $3a_2 \rightarrow 7b_2$ transitions in $Re_2Cl_4(PH_3)_4$, with the calculated singlet energies ~2000 cm^{-1} higher than the OED's listed in Table II. Extensive transition-state calculations that we have performed on $[Re_2Cl_8]^{2-}$ [15] and $Cr_2(O_2CH)_4 \cdot 2H_2O$,[23] demonstrate a uniform shift to higher energies for the singlet relative to OED transition energies—regardless of the type of orbital transition! There is, however, considerable variation in the singlet–triplet separations, with metal-to-metal transitions generally having larger values (~2000–3000 cm^{-1}) than LMCT excitations. We, therefore, consider it justified to use OED's instead of the much more expensive transition-state energies, particularly when the quantitative agreement is not going to be considered a critical factor. Therefore, any numerical agreement between the experimental and OED transition energies is fortuitous, as the singlet transition-state energies are expected to be ~2000 cm^{-1} higher, but the relative spacings and qualitative agreement are quite real.

The Re–Re stretching frequency in the $^2B_2$ excited state resulting from the $\delta \rightarrow \delta^*$ transition in $[Re_2Cl_4(PPr_3)_4]^+$ was found to be 275 ± 5 cm^{-1}. This value, when compared to the excited-state $\delta \rightarrow \delta^*$ value of 248 cm^{-1} [24] in $[Re_2Cl_8]^{2-}$, implies a stronger excited-state and, by analogy, ground-state, Re–Re metal bonding interaction in $[Re_2Cl_4(PR_3)_4]^+$ than that in $[Re_2Cl_8]^{2-}$. This is consistent with the relative stability of the Re–Re σ-bonding level in the Xα-SW calculations on $[Re_2Cl_4(PH_3)_4]^{0,1+}$. Another comparison is with the ground state M–M frequency of 274 cm^{-1} [25] in $[Re_2Cl_8]^{2-}$, which further suggests that the metal–metal bonding in the quadruply bonded configuration $\sigma^2\pi^4\delta^2$ (bond order of 4), of $[Re_2Cl_8]^{2-}$ is similar in strength to that in $[Re_2Cl_4(PH_3)_4]^+$ which has a $\sigma^2\pi^4\delta^1\delta^{*2}$ (bond order of 2.5) excited-state configuration. Upon completion of some structural studies of $[Re_2Cl_4(PR_3)_4]^n$, $n = 0, 1+, 2+$ we shall be in a position to discuss these relationships in more detail.

Acknowledgment. This research was generously supported by the National Science Foundation and by the Robert A. Welch Foundation.

Registry No. $Re_2Cl_4(P(n\text{-}Pr)_3)_4$, 52359-07-6; $[Re_2Cl_4(P(n\text{-}Pr)_3)_4]PF_6$, 76897-96-6; $Re_2Cl_4(PH_3)_4$, 76521-83-0.

(23) Bursten, B. E.; Cotton, F. A.; Stanley, G. G., unpublished results.
(24) Cowman, C. D.; Gray, H. B. *Inorg. Chem.* **1973**, *98*, 8177.
(25) Bratton, W. K.; Cotton, F. A., Debeau, M.; Walton, R. A. *J. Coord. Chem.* **1971**, *1*, 121.